Molecular Interactions between Estrogen Receptor and Its Ligand Studied by the ab Initio Fragment Molecular Orbital Method

Kaori Fukuzawa,*,†,‡ Yuji Mochizuki,‡,§,& Shigenori Tanaka,‡,|| Kazuo Kitaura,‡,⊥ and Tatsuya Nakano‡,#

Mizuho Information and Research Institute, Inc., 2-3 Kanda Nishiki-cho, Chiyoda-ku, Tokyo 101-8443, Japan, Japan Science and Technology Agency, CREST, Advancesoft and Institute of Industrial Science, Center for Collaborative Research, The University of Tokyo, 4-6-1 Komaba, Meguro-ku, Tokyo 153-8904, Japan, Graduate School of Science and Technology, Kobe University, 1-1, Rokkodai, Nada, Kobe 657-8501, Japan, National Institute of Advanced Industrial Science and Technology, 1-1-1 Umezono, Tsukuba, Ibaraki 305-8568, Japan, and Division of Safety Information on Drugs, Food, and Chemicals, National Institute of Health Sciences, 1-18-1 Kamiyoga, Setagaya-ku, Tokyo 158-8501, Japan

Received: February 6, 2006; In Final Form: May 19, 2006

The ab initio fragment molecular orbital calculations were performed for molecular interactions of the whole estrogen receptor (ER) ligand-binding domain with a natural ligand, 17β-estradiol (EST). The interaction energies of the ligand at the residue level were calculated using HF and MP2 methods with several basis sets. The charge-transfer (CT) interactions were also analyzed based on configuration analysis for fragment interaction. Strong electrostatic interactions were observed between the EST and surrounding charged/polarized residues, Glu353, Arg394, His524, and Thr347. Weak electrostatic and significant van der Waals dispersion interactions were observed between the EST and the many surrounding hydrophobic residues. Together with the experimental interpretations, both interactions equally contributed to the total binding energies, and it was found that the inclusion of electron correlation was essential to obtain an appropriate picture of the interaction. The strongest interaction energy was observed between Glu353 and the EST, and the CT interactions from the lone-pair orbital of the carbonyl oxygen of Glu353 to the σ^*_{OH} orbital of the hydroxyl group of EST were found to be important. The CT interactions from the lone-pair orbital of EST to the σ^*_{NH} of Arg394 and from the lone-pair orbital of EST to the σ^*_{NH} of His524 were also observed. These CT interactions occurred through the hydrogen-bond networks between the ER and EST. Therefore, electron donations from the ER to the EST and electron back-donations from EST to the ER were characteristic of ER−ligand binding. Our approach provides a powerful tool to understanding detailed molecular interactions at the quantum mechanical level.

1. Introduction

The estrogen receptor (ER) is a member of the nuclear receptor (NR) superfamily that acts as a ligand-activated transcription factor. Its endogenous ligands are steroid hormone estrogens, and these hormones play important roles in the regulation of growth, differentiation, and homeostasis in a variety of tissues. The functions of ER are induced by the binding of estrogens to the ER ligand-binding domain (LBD).[1,2] As well as the naturally occurring estrogens, it is known that a variety of compounds such as medical compounds and endocrine disruptors might bind to the ER and lead to estrogenic activities.[3,4] In particular, the ER is linked to diseases such as breast cancer, endometrial cancer, and osteoporosis, and the ER has therefore been one of the most important targets for the development of therapeutic agents and screening of environmental pollutants. One well-established methodology for the screening of candidate compounds is a receptor-binding assay based on binding affinities to the ER, and in silico screening has also recently been performed to predict binding affinities. To perform efficient screening, it is necessary to understand the binding mechanism of the ER with ligands.

The structural details of ER−ligand binding have been revealed by X-ray crystal structure analysis. Figure 1 shows the crystal structures for the complex of human ER-LBD and xenoestrogen, 17β-estradiol (EST).[5,6] The EST as an agonist binds to the "ligand-binding pocket" of the ER; the EST is surrounded by some charged/polarized residues and a number of hydrophobic residues. On the basis of these structural data, it is known that some important charged/polarized residues, Glu353, Arg394, and His524, exist at the ligand-binding site of the ER and they construct hydrogen-bond networks with the ligand directly or through the mediation of a single water molecule (Figure 2). These hydrogen bonds are thought to play a key role in ER−ligand binding, but the details of their contributions to this binding remain to be elucidated. Furthermore, the roles of other surrounding residues and distant residues in the ER-LBD also remain unclear. Experimental mutagenesis has also been reported to analyze the function of distinct amino acid residues in the ER.[7] Each single point mutation at Glu353, Gly521, His524, Leu525, and Met528 was found to reduce estrogen binding, and these findings indicated the "direct" and "indirect" interactions between ligand and these residues.

Computational simulations for ER−ligand complexes are anticipated to provide detailed information regarding the binding

* Author to whom correspondence should be addressed. Phone: +81-3-5281-5271. Fax: +81-3-5281-5414. E-mail: kaori.fukuzawa@gene.mizuho-ir.co.jp.
† Mizuho Information and Research Institute, Inc.
‡ Japan Science and Technology Agency, CREST.
§ Advancesoft and The University of Tokyo.
|| Kobe University.
⊥ National Institute of Advanced Industrial Science and Technology.
National Institute of Health Sciences.
& Present address: Department of Chemistry, Faculty of Science, Rikkyo University, 3-34-1 Nishi-ikebukuro, Toshimaku, Tokyo 171-8501, Japan.

10.1021/jp060770i CCC: $33.50
Published on Web 07/21/2006

Figure 1. Structure of the ER−EST complex. The illustration was provided by DS Viewer Pro 5.0, Accelrys, Inc.

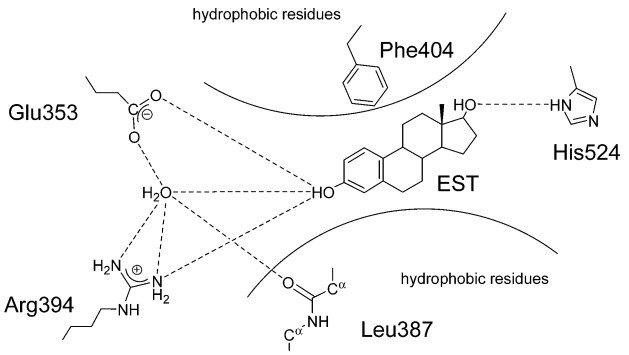

Figure 2. Hydrogen-bond networks at the ligand-binding site of ER complexed with EST. Dotted lines indicate hydrogen bonds.

mechanism and interactions of interest. A number of theoretical studies have been carried out to clarify the mechanism of ER−ligand binding.[8,9] Although most calculations carried out to date have employed classical mechanical methods based on empirical force fields, such methods remain limited with respect to obtaining an accurate analysis of intermolecular interactions such as charge redistribution and charge-transfer (CT) interactions. In contrast to the limitations of such classical approaches to molecular simulation, quantum mechanical simulations have been used to successfully characterize weak intermolecular interactions and CT processes. Because several different types of interactions are involved in ER−ligand interactions, quantum mechanical treatment is necessary to obtain an accurate and systematic understanding of these interactions.

We have previously performed quantum mechanical calculations for the binding energies of ER with several ligands[10] based on the ab initio fragment molecular orbital (FMO) method[11−14] at the Hartree−Fock (HF) level with the STO-3G minimal basis set (HF/STO-3G). We found the calculated relative binding energies to be in good correlation with the experimental relative binding affinities. We also found the ER−ligand interaction to be properly described by considering the amino acid residues in the first layer of α-helices around the ligand. These findings indicated the possibility of using this approach for in silico screening. In addition, it was found that the binding energy is related to charges transferred from the ER to the ligand; as the transferred charge increases, the binding energy also becomes larger. The decrease in negative charges on Glu353 is particularly significant, and its amount was found to be nearly equal to the increase in negative charge on the ligand. Therefore, it was supposed that the CT interactions between ER and ligand are important to their binding. To better understand the details of this binding mechanism, higher-level calculations and detailed analysis of the interactions between the ligand and individual amino acid residues as well as the CT interactions concerning hydrogen bonding are required.

The FMO method[11−14] and the ABINIT-MP program package[15] have been developed for accurate analysis of biomacromolecules. The interfragment interaction energies (IFIEs)[16−18] between single and multiple fragments can be evaluated by FMO calculations. The IFIEs are calculated for all fragment pairs, and the sum of these IFIEs can be assumed to be the interaction energies between selected fragments. Using IFIE analysis, interactions at a residue level (ligand−residue and residue−residue interactions) can be estimated when the fragmentations are performed according to the amino acid unit for the protein. We have recently developed electron-correlation methods beyond the HF method such as the second-order Møller−Plesset perturbation (MP2) method[19−21] for use with the FMO procedure. We have already applied the MP2 method in several biomacromolecular investigations: Molecular interactions between cyclic AMP receptor protein and DNA[18] have been investigated, and binding energies of the peroxisome-proliferator-activated receptor γ (PPAR-γ)[23] with specific ligands have been calculated. In former studies using the MP2 method, our results have suggested that dispersion energies play an important role in interactions among biomacromolecules. We have also recently developed a configuration analysis for the fragment interaction (CAFI)[24,25] method to analyze the CT interactions associated with hydrogen bonding. In the CAFI method, the orbital interactions can be distinguished between the CT and the polarization (POL), and interactions can be estimated at an orbital level.

In the present study, we applied recently developed FMO methods to a detailed analysis of the ER−ligand complex system. We performed HF calculations with several basis sets, in addition to the STO-3G level used in our former study.[10] We also performed MP2 calculations for more accurate analysis and compared investigation for all levels of calculations. With these levels of theory, the IFIE analysis was performed for interactions between ligands and individual amino acid residues; ligand interactions with both charged/polarized residues and hydrophobic residues were investigated. Furthermore, we analyzed differences in charge distribution and electron densities between the ER−ligand complex and individual component molecules. We also analyzed the CT interactions in hydrogen-bond networks between ERs and ligands, using the CAFI method. We thus addressed the intermolecular interactions between ERs and ligands at a residue level and CT interactions at an orbital level.

2. Theoretical Calculations

The initial atomic coordinates of the ER−EST complex were obtained from the Protein Data Bank (PDB),[5] PDB code 1ERE.[6] On the basis of this structure, the entire LBD of the receptor protein (residues 307−547), EST, and a water molecule were selected for simulations. The number of atoms in the complex is 3946, including hydrogen atoms. The geometry of the ER−EST complex used for the FMO calculations was the same as in our previous HF/STO-3G study (MODEL 1 in the ref 21), and the geometries of free ER and EST were fixed at the complexed geometries; the modeling details are described in ref 21. With these geometries, the ab initio FMO[11−14] calcula-

tions were carried out under gas-phase conditions at the HF level with STO-3G, 6-31G, 6-31G*, and 6-31G** basis sets. The energies and electron densities were further improved at the MP2 level[19,20] with 6-31G and 6-31G* basis sets. The approximations of electrostatic potentials[14] considered as the Mulliken orbital charge (esp-aoc) and the fractional point charge (esp-ptc) were carried out when the distance between the closest contact atoms in the two fragments exceeds 0.0 and 2.0 in units of van der Waals radii (vdW), respectively. In addition, the Coulomb interaction approximation (dimer-es)[14] was applied for the fragment pair calculations in two fragments with separations exceeding 2.0 in the same vdW units. These approximations have reduced the computational time by about several times at the sacrifice of the enhanced error in total energy by about several kcal/mol. Especially, the esp-aoc approximation with the 0.0 threshold would affect the total energy, while the error in the relative energies is expected to be of smaller order of magnitude. The fragmentation of the system was as follows: Each amino acid residue of ER, the EST molecule, and the water molecule were treated as a single fragment.

The IFIE[16−18] in FMO calculations is defined as follows

$$\Delta E_{IJ} = (E'_{IJ} - E'_{I} - E'_{J}) + \mathrm{Tr}(\Delta \mathbf{P}^{IJ}\mathbf{V}^{IJ}) \qquad (1)$$

where $\Delta\mathbf{P}^{IJ}$ is a difference density matrix, $\mathbf{V}^{IJ}$ is an environmental electrostatic potential for fragment dimer IJ from other fragments, and E'_{I} and E'_{IJ} are energies of fragment monomer I and dimer IJ without environmental electrostatic potential. The many-body effects are considered through the environmental electrostatic potentials. From ΔE_{IJ}, the total energy E is calculated by

$$E = \sum_{I>J} \Delta E_{IJ} + \sum_{I} E'_{I} \qquad (2)$$

The IFIEs in the ER−EST complexes, primarily for the ligand−residue interactions, were analyzed and compared at each level of theory. The effect of the esp approximations on the IFIE is expected to be of a smaller order of magnitude than that on the total energy because only the second term of the eq 1, which contains $\Delta\mathbf{P}^{IJ}$, is affected by the influence of the electrostatic potential.

In the CAFI calculations,[24,25] we used a small model molecule, MODEL 3 of ref 10. This model consists of a ligand, a water molecule, the side chains of the residues Glu353, Arg394, and His524, and the main chain of Leu387, which construct hydrogen-bond networks with the ligand (Figure 2). The geometry of MODEL 3 was optimized at the conventional HF/6-31G* level with the backbone atoms fixed at the positions given in MODEL 1. The Gaussian03 program package[26] was used for the optimizations. The FMO−CAFI calculations were carried out at the HF/6-31G* level. The weight parameters for the virtual space in the weighted Löwdin orthonormalization (WLO)[25] were 0.07.

All the FMO calculations were performed with the ABINIT-MP program,[15] and the visualization was carried out with a BioStation Viewer.[27] The calculations were performed on 16 Dual Xeon 3.06 GHz clusters (32 CPUs), 8 Dual Xeon 2.2 GHz clusters (16 CPUs), and 32 Dual AMD Opteron 2.0 GHz clusters (64 CPUs). The time elapses for calculations of the ER−EST complex at the MP2/6-31G* level with electron densities were 100.7 h by the Opteron clusters. In the following section, we discuss the results calculated at the MP2/6-31G* level of theory, unless otherwise stated.

TABLE 1: Binding Energies (ΔE)[10] and IFIEs of Several Ligands with the ER Calculated by the HF/STO-3G Method[a]

	binding energies[b]	IFIEs	
ligand	ΔE	1 residue unit[c]	2 residue unit[b]
17β-estradiol	−37.65	−42.46	−42.78
diethylstilbestrol	−28.33	−33.16	−32.31
raloxifene	−26.13	−33.97	−34.12
4-hydroxytamoxifen	−38.19	−45.69	−45.13

[a] Energies are in kcal/mol. [b] Fragmentations were in 2 residue units. [c] Fragmentations were in 1 residue units.

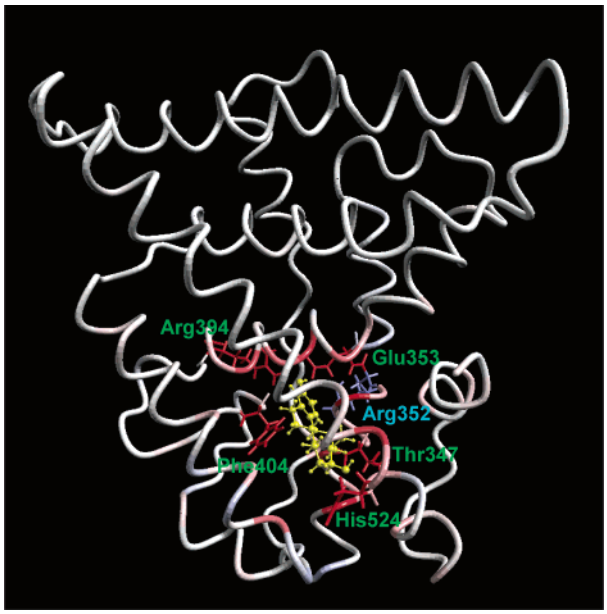

Figure 3. Visualization of the IFIEs between the EST and each amino acid residue fragment of the ER calculated at the MP2/6-31G* level. The ball-and-stick, stick, and line representations refer to EST and a water molecule, residues with strong interactions, and ER, respectively. The color represents the sign and strength of the interactions between the fragments. In the domain indicated in yellow (EST), the red and blue fragments illustrate stabilized and destabilized interactions, respectively, and the deepness of the hue indicates the strength of the interaction.

3. Results and Discussion

First, we confirmed the reliability of IFIE analysis for ER−ligand interactions at the HF/STO-3G level. The sum of all the IFIEs between the ligand and each fragment in the ER could be assumed to be the interaction energy between the ligand and the ER. Such IFIEs for four ligands, 17β-estradiol, diethylstilbestrol, raloxifene, and 4-hydroxytamoxifen, were compared with ER−ligand binding energies (ΔE), as determined by conventional supermolecular calculations with fixed geometries[10] (Table 1). The differences between the ΔE values and IFIEs are due to the electron density deformation of the individual molecules in their complex.[17] The corresponding deformation energies were of several kcal/mol, which were common among all the calculations. Therefore, we concluded that the relative IFIE values for each ligand were comparable to those of ΔE. In addition, we examined the errors of IFIEs obtained between two fragmentations of ER, one and two residues per fragment. The discrepancies of the sum of the IFIEs between the two fragmentations were less than 1 kcal/mol. Therefore, at least qualitative understanding could be obtained by IFIE analysis with the smaller fragmentation, and residue−ligand and residue−residue interactions could then be estimated.

3.1. Ligand Interactions with Charged/Polarized Residues. Figure 3 illustrates the strength of the interactions of EST with

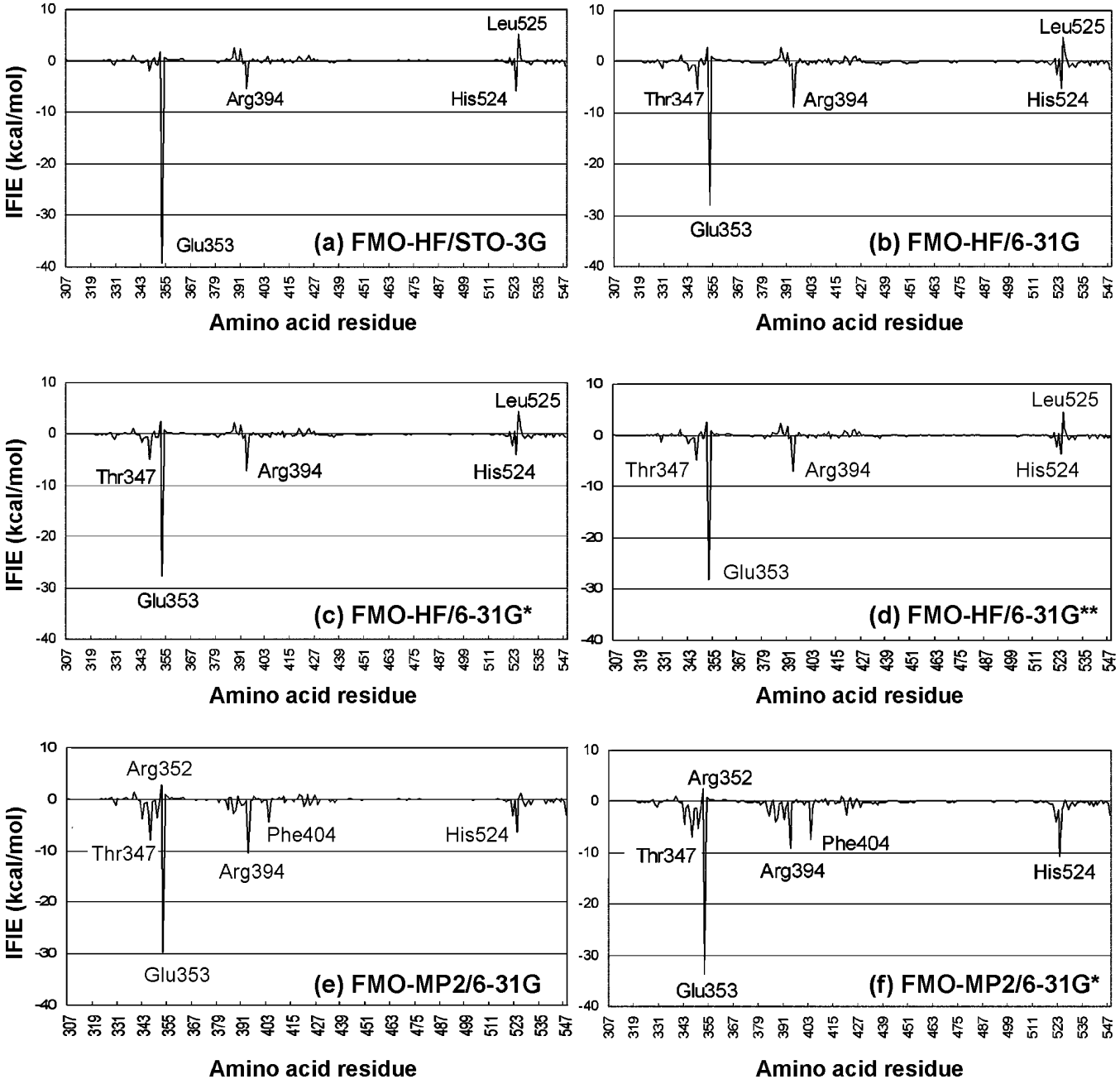

Figure 4. IFIEs between the EST and each amino acid residue fragment.

each residue fragment of the ER according to color at the MP2/6-31G* level. All colored residues with strong interaction were geometrically located around the EST. In particular, Glu353, His524, Arg394, Phe404, and Thr347 indicated stabilized interactions, and Arg352 indicated destabilized interactions. These findings support discussions in our previous study[10] that the relative binding energies of the ER−ligand complexes are properly described by considering a model protein with the first layer of α-helices around the ligand.

Figure 4 shows numerical representations of Figure 3 for the same and several different calculations, and the stronger interactions are also listed in Table 2. The remarkably stabilized residue was Glu353 throughout all levels of calculations, with IFIEs from −27.8 to −39.3 kcal/mol. Arg394, His524, and Thr347 were also found to have stronger stabilization at any level, i.e., from −5.3 to −10.5, from −3.6 to −10.7, and from −1.9 to −8.0, kcal/mol, respectively; the MP2 level led to stronger interactions, and the HF/STO-3G level except for Glu353 led to weaker interactions as compared to the other methods. All of these residues were charged or polarized, which induced electrostatic interactions with the ligand. In particular, Glu353, Arg394, and His524 are known to construct a hydrogen-bond network with EST at the ligand-binding site of the ER (Figure 2). Therefore, one factor in the creation of such large IFIEs is the hydrogen bonds between the residues. However, a destabilized fragment with considerable IFIE values was Arg352 within the charged/polarized residues, i.e., 2.4−2.7 kcal/mol, except for the STO-3G level which had a smaller value (1.8 kcal/mol). Experimental mutagenesis[7] suggested that the single point mutations at Glu353 and His524 induced a decrease of estrogen binding. Together with the IFIE results, therefore, strong interactions between ligand and these residues with the hydrogen bonds play a key role in the ER−ligand binding.

Whereas all of the HF levels of the method applied here gave qualitatively similar results for charged/polarized residues, the minimal basis set, STO-3G, overestimated the IFIEs of the

TABLE 2: IFIEs between EST and Each Amino Acid Residue of the ER[a]

method	HF								MP2			
basis set	STO-3G		6-31G		6-31G*		6-31G**		6-31G		6-31G*	
attractive interactions	Glu353	−39.28	Glu353	−27.92	Glu353	−27.75	Glu353	−28.19	Glu353	−29.83	Glu353	−33.77
	His524	−5.98	Arg394	−8.75	Arg394	−7.10	Arg394	−7.00	Arg394	−10.47	His524	−10.71
	Arg394	−5.27	Thr347	−5.41	Thr347	−5.04	Thr347	−4.87	Thr347	−7.97	Arg394	−9.10
	Thr347	−1.92	His524	−5.26	His524	−3.89	His524	−3.61	His524	−6.29	**Phe404**	**−7.48**
	water	−1.02	**Met522**	**−2.44**	**Met522**	**−2.21**	**Met522**	**−2.19**	**Phe404**	**−4.46**	Thr347	−7.02
	Glu330	−0.92	**Met343**	**−1.85**	**Met343**	**−1.58**	**Met343**	**−1.57**	**Met343**	**−3.70**	**Ala350**	**−5.20**
	Met522	**−0.82**	water	−1.59	Glu330	−1.20	Glu330	−1.17	**Leu346**	**−3.58**	**Met343**	**−4.43**
	Lys531	−0.74	Glu330	−1.27	Lys531	−0.92	Lys531	−0.87	**Ala350**	**−3.56**	**Leu346**	**−4.34**
	Asp351	−0.71	Lys531	−1.02	**Met528**	**−0.91**	**Met528**	**−0.83**	**Met522**	**−3.26**	**Leu387**	**−4.06**
	Val392	**−0.66**	**Met528**	**−1.02**	**Gly344**	**−0.84**	**Gly344**	**−0.79**	water	−2.90	**Met522**	**−3.92**
	Ala350	**−0.64**	**Gly344**	**−1.00**	**Val392**	**−0.78**	**Val392**	**−0.74**	**Leu387**	**−2.74**	**Leu391**	**−3.61**
	Glu542	−0.51	**Val392**	**−0.89**	Asp538	−0.74	Asp538	−0.73	**Met388**	**−2.21**	**Met388**	**−3.10**
	Ala405	**−0.49**	Asp538	−0.77	Glu542	−0.69	Glu542	−0.68	**Leu384**	**−1.93**	**Leu384**	**−2.77**
	Asp538	−0.47	**Ala350**	**−0.74**	**Ala350**	**−0.66**	**Ala350**	**−0.62**	**Met528**	**−1.43**	**Met421**	**−2.67**
	Glu380	−0.45	Glu542	−0.72	Arg412	−0.62	Arg412	−0.61	**Met421**	**−1.37**	water	−2.48
	Arg412	−0.44	**Leu346**	**−0.72**	**Leu346**	**−0.61**	Arg436	−0.60	Glu330	−1.27	Glu523	−1.66
	Lys529	−0.38	Glu380	−0.67	Glu380	−0.61	Glu380	−0.60	**Leu391**	**−1.18**	**Met528**	**−1.61**
	Gly344	**−0.38**	Arg436	−0.62	Arg436	−0.60	Asp351	−0.57	**Ile424**	**−1.17**	**Leu525**	**−1.54**
repulsive interactions	Arg352	1.83	**Leu391**	**1.79**	**Leu391**	**1.68**	**Leu391**	**1.70**	Glu419	1.00	Glu423	0.90
	Leu391	**2.35**	Arg352	2.69	**Met388**	**2.38**	**Met388**	**2.35**	Tyr526	1.05	Glu419	0.95
	Met388	**2.51**	**Met388**	**2.76**	Arg352	2.52	Arg352	2.43	Glu339	1.25	Glu339	1.11
	Leu525	**5.15**	**Leu525**	**4.64**	**Leu525**	**4.41**	**Leu525**	**4.53**	Arg352	2.69	Arg352	2.52
[b]charged/polarized	−54.48		−50.42		−45.42		−45.11		−60.18		−70.77	
[c]**hydrophobic**	**12.02**		**4.95**		**5.15**		**5.77**		**−32.99**		**−52.96**	
[d]total	−42.46		−45.48		−40.26		−39.34		−93.17		−123.73	

[a] Only selected values with stronger interactions are shown, and they are listed in order of the interaction energy values. Energies are in kcal/mol. Hydrophobic residues are indicated as bold characters. [b] Sum of all IFIEs between EST and each charged or polarized residue in the ER.[c] Sum of all IFIEs between EST and each hydrophobic residue in the ER. [d] Sum of all IFIEs between EST and each residue in the ER.

strongest interactions for both the stabilized and the destabilized residues mentioned above. In contrast, IFIEs of weaker interactions were underestimated at this level. Thus interactions with the EST were localized on specific residues when they were calculated at the HF/STO-3G level. At least double-ζ treatment was necessary to obtain an overall picture of the electrostatic interactions. In addition, inclusion of the electron correlation at MP2 levels led to more stabilized interactions with most of the charged/polarized residues. The sums of IFIEs between the ligand and each charged/polarized residue were −54.5, −50.4, −45.4, −45.1, −60.2, and −70.8 kcal/mol for the HF/STO-3G, 6-31G, 6-31G*, 6-31G**, MP2/6-31G, and 6-31G* levels, respectively, although expansions of basis sets in the HF methods reduced the interaction energies and the MP2 results gave more stabilized energies, all of which indicated a "stabilized" character.

3.2. Ligand Interactions with Hydrophobic Residues. While charged and polarized residues either strongly or weakly interacted with the ligand, hydrophobic residues also contributed to weak interactions. Further, while the IFIEs of charged and polarized residues were qualitatively similar between both the HF and the MP2 methods, those of the hydrophobic residues were different according to these methods. In the HF method, except with the STO-3G basis set, Met522 and Met343 were stabilized from −2.2 to −2.4 and from −1.6 to −1.9 kcal/mol, respectively, Leu525, Met388, and Leu391 were destabilized by 4.4−4.6, 2.4−2.8, and 1.7−1.8 kcal/mol, respectively, and many residues were either slightly stabilized or destabilized. In the HF methods, the sum of the IFIEs between the ligand and each hydrophobic residue were similar, 4.9−5.2 kcal/mol, except with the STO-3G basis set which had a larger value (12.0 kcal/mol); all sums showed positive values (repulsive interactions). However, at the MP2 level with the 6-31G and 6-31G* basis sets, the sums of the IFIEs were large negative values (attractive interaction), −33.0 and −53.0 kcal/mol, respectively. Many hydrophobic residues were found to be stabilized through electron correlations. The stabilization of Phe404 was especially significant, −4.5 and −7.5 kcal/mol with the 6-31G and 6-31G* basis sets, respectively, as compared to the HF results from −0.13 to +0.91 kcal/mol. The side-chain phenyl group of Phe404 is located perpendicular to the steroid A and B rings of the ligand, and these moieties construct T-shape $\pi-\pi$ interactions (Figure 3). Also, the change of interaction energy was remarkable for Leu525, repulsive by 4.4−5.2 kcal/mol at the HF levels and attractive by −1.5 kcal/mol at the MP2/6-31G* level. The experimental mutagenesis,[7] again, suggested that single point mutations at Gly521, Leu525, and Met528 induced a decrease of estrogen binding. Such results supported the stabilized interaction between Leu525 and the EST. Met528 was stabilized at all levels of calculations, and Gly521 was found to be slightly destabilized, 0.51−0.56 kcal/mol at the HF levels and 0.03 kcal/mol at the MP2/6-31G level, but slightly stabilized, −0.88 kcal/mol, at the MP2/6-31G* level. These findings suggest "direct" interactions between the ligand and these hydrophobic residues that were important for the binding function of the ER. (Data for smaller values in the discussions above are not shown in Table 2.)

Figure 5 shows the hydrophobic residues that interacted with the ligand stronger than ±1 kcal/mol at both the HF/6-31G* and MP2/6-31G* levels, and all of them were located around the ligand. In the HF/6-31G* method, some hydrophobic residues were visualized as either stabilized or destabilized. In contrast, in the MP2/6-31G* method, many hydrophobic residues appeared to be stabilized, and fewer of them appeared to be destabilized. Almost all hydrophobic residues surrounding the ligand were found to be stabilized, and none was destabilized by more than 1 kcal/mol. These stabilizations were dominated by the van der Waals dispersion interactions that could be considered by electron-correlation methods. As typified by the $\pi-\pi$ interaction with Phe404, weak but numerous interactions with these hydrophobic residues significantly stabilized the ER−ligand binding more than those obtained by the HF method.

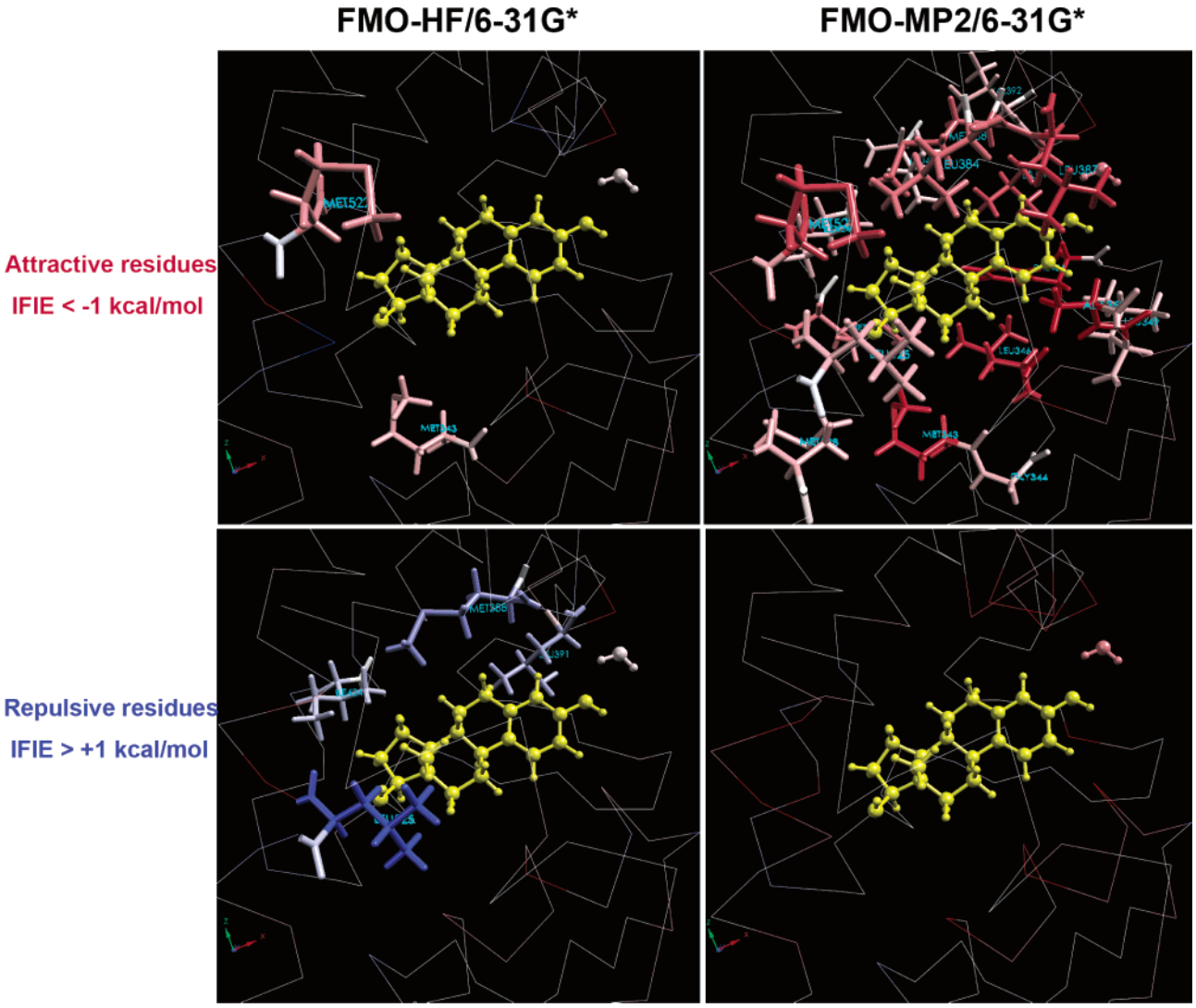

Figure 5. Hydrophobic residues that showed IFIE values with the EST stronger than ±1 kcal/mol: left, at the HF/6-31G* level; right, at the MP2/6-31G* level. The ball-and-stick representation refers to EST and a water molecule; the stick representation refers to hydrophobic residues with significant IFIE values. The line representation is the Cα backbone. In the domain indicated in yellow (EST), the red and blue fragments illustrate stabilized and destabilized interactions, respectively, and the deepness of the hue indicates the strength of the interaction.

3.3. ER−Ligand Interaction Energies. The total IFIEs between the ligand and all residues of the ER were −42.5, −45.5, −40.3, and −39.3 kcal/mol at the HF/STO-3G, 6-31G, 6-31G*, and 6-31G** levels, respectively, and much larger in magnitude, −93.2 and −123.7 kcal/mol, at the MP2/6-31G and 6-31G* levels. The van der Waals dispersion interactions were equally significant as compared to the electrostatic interactions. These findings suggest that the electron correlation is essential to characterizing the ligand interactions at the hydrophobic binding pocket. The large energy difference between the HF and the MP2 methods was due to the dispersion interaction. The energy difference of 30 kcal/mol still existed between the MP2/6-31G and 6-31G* levels, suggesting that the interaction energies were not converged yet. Hobza's group[28−30] has suggested the importance of a high-level electron-correlation method with a large basis set, such as CCSD(T) with the complete basis set (CBS) limit, for hydrogen-bonding and stacking systems. However, they have also suggested that interaction energies calculated at the MP2/6-31G* level were qualitatively similar to those at the CCSD(T) levels, with errors of ∼10% for hydrogen-bond interactions and ∼20% for stacking interactions.[18,28−30] Because such higher-level of calculations are formidable by current computational resources for the whole ER−ligand complex, we qualitatively discussed the MP2/6-31G* results.

An empirical study for the binding affinity between the ER and the EST was performed by Lipzig et al.[9] using the Amber force field. The ligand-binding energy to ER (ΔE_{ER}) and the ligand solvation energy (ΔE_{SOL}) were decomposed to the electrostatic (E^{EL}) and van der Waals (E^{VDW}) energies: E^{EL} and E^{VDW} were from −27.1 to −27.5 and from −38.4 to −39.6 kcal/mol, respectively, for ΔE_{ER} at dominant ligand orientations and −32.7 and −23.1 kcal/mol, respectively, for ΔE_{SOL}. The ΔE_{ER} values were about −66 kcal/mol, which were of the same order of magnitude as our total IFIE values. Further, similar weights of E^{EL} and E^{VDW} in ΔE_{ER} were consistent with our IFIE results that charged/polarized and hydrophobic residues were equally significant. The empirical binding energy in solution, $\Delta E_{ER} - \Delta E_{SOL}$, was about −10 kcal/mol. Similar solvation energies are expected also in the FMO calculation, and therefore, cancellation between binding energy to the ER and desolvation energy would take place to produce a much smaller binding energy in solution than the current IFIE value of −120 kcal/mol. Although our previous study reported that the FMO relative binding energies in the gas phase were well correlated with the experimental relative binding affinities,[10]

desolvation effects should be considered when we discuss the absolute binding energies. Such a FMO calculation with desolvation effects will be the subject of our future investigations.

3.4. Charge-Transfer Interactions. We have previously suggested[21] that for several different ligands the negative charges transferred from the ER to the ligands upon binding are related to their binding energies; the binding energy increases with increases in the negative charge of the ligand. Further, similar amounts of positive charge were induced on Glu353. It was therefore thought that CT occurred from the Glu353 to the ligand and that the CT interactions could be a major controlling factor of ER−ligand binding.

Here, we calculated differences in the net atomic charges (Δq) between the ER−EST complex and the individual component molecules with fixed geometries at the MP2/6-31G* level. The Δq between the free and the complexed forms is defined by the following equation

$$\Delta q = q(\text{complex}) - (q(\text{ER}) + q(\text{EST})) \qquad (3)$$

where q(ER), q(EST), and q(complex) are the total charges of each residue in free ER, those of the free EST, and those of each residue and the ligand in the complex, respectively. The Δq for Glu353 indicated a large positive value, 0.129e, and that for EST indicated a similar negative value, −0.114e. Those for Arg394 and His524 also indicated small negative values, −0.020e and −0.036e, respectively. The Δq for Thr347 was much smaller, 0.008e, and this residue was therefore thought to have a lesser contribution to the CT interaction. At the HF/6-31G* level, Δq values for Glu353, EST, Arg394, His524, and Thr347 were 0.097e, −0.095e, −0.017e, −0.007e, and 0.008e, respectively. Δq values tended to be smaller in magnitude compared with MP2 values, and the inclusion of electron correlation therefore seems to enhance the CT character.

The differences in electron densities ($\Delta\rho$) between the free and complexed forms are also calculated at the MP2/6-31G* level. $\Delta\rho$ is defined by a similar equation

$$\Delta\rho = \rho(\text{complex}) - (\rho(\text{ER}) + \rho(\text{EST})) \qquad (4)$$

where ρ(ER), ρ(EST), and ρ(complex) are electron densities on three-dimensional grids for the free ER, free ligand, and their complex, respectively. As shown in Figure 6, remarkable distributions of $\Delta\rho$ were observed only around the EST. The distributions were particularly significant at the EST−Glu353 interaction site, and some of them were observed at the EST−His524 and EST−Arg394 interaction sites. Both results for Δq and $\Delta\rho$ gave similar tendencies.

The CAFI calculations[25] were carried out at the HF/6-31G* level to consider CT interactions between the ER and the EST at an orbital level. The CT and POL energies among fragments (CPEF) obtained in the CAFI calculations are listed in Table 3, where interaction energies are shown with donor−acceptor directions. Note that absolute energy values in the CPEF table depended on the WLO parameters,[25] so only qualitative discussions are possible. We use the abbreviation "from → to" in the following discussion. The strongest CT interactions were observed in Glu353 → EST, −19.8 kcal/mol. Together with the opposite "back CT", EST → Glu353 interaction of −0.9 kcal/mol, the total interaction energy between Glu353 and EST was −20.7 kcal/mol. This total energy corresponded to the IFIE between them, −27.8 kcal/mol, at the HF/6-31G* level, and these differences can be attributed to the electrostatic interaction that could not be described in the CAFI method. The second-strongest CT interaction was water → Arg394, −14.1 kcal/mol,

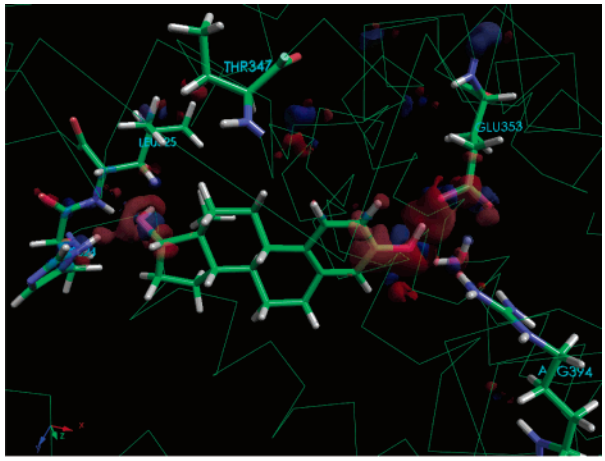

Figure 6. Difference in electron densities ($\Delta\rho$) between complexed and individual component molecules; $\Delta\rho = \rho(\text{complex}) - (\rho(\text{ER}) + \rho(\text{ligand}))$ calculated at the MP2/6-31G* level. The stick representation refers to EST, a water molecule, and residues (Glu353, Thr347, Arg394, His524, and Leu525) with significant $\Delta\rho$ values. The line representation is the Cα backbone. The red (minus) and blue (plus) represent the sign of the isosurfaces at ±0.003e/bohr^3.

TABLE 3: CAFI Energies[a]

	to					
from	Glu353	His524	Leu387	Arg394	EST	water
Glu353	−0.107	0.000	−0.001	−0.525	−19.792	−9.626
His524	0.000	−0.295	0.000	0.000	−1.045	0.000
Leu387	−0.001	0.000	−0.063	−0.067	−1.317	−4.281
Arg394	−0.031	0.000	−0.013	−2.750	−0.633	−0.373
EST	−0.870	−5.299	−0.432	−7.090	−3.168	−0.808
water	−0.627	0.000	−1.685	−14.138	−0.355	−1.171

[a] Energies are in kcal/mol.

and the back CT Arg394 → water interaction was −0.37 kcal/mol. Strong CT interactions were also observed in Glu353 → water (−9.6 kcal/mol), EST → Arg394 (−7.1 kcal/mol), EST → His524 (−5.3 kcal/mol), and Leu387 → water (−4.3 kcal/mol). Some POL interactions were observed at EST, Arg394, and water of −3.2, −2.8, and −1.2 kcal/mol, respectively. Several CT interactions weaker than those discussed above existed, including back CTs such as water → Leu387 and His524 → EST interactions. These observations clearly explain the strength and the direction of hydrogen-bond networks in the ligand-binding site of the ER shown in Figure 2; these hydrogen bonds occur directly between the ligand and the surrounding residues as well as through the mediation of a single water molecule.

The pair of donor−acceptor orbitals is visualized in Figure 7. Here, the numbering corresponds to the order of the strengths of the interactions; only interactions between the EST and the ER were focused on, and the others were either residue−residue or residue−water interactions. The strongest pair, "1", was the CT interaction from the lone-pair orbital of the carbonyl oxygen with π-character, $n_O(\pi)$, of Glu353 to the σ^*_{OH} orbital of the hydroxyl group of EST, and the occupation number of the transferred electron was 0.0161. We defined the abbreviation for this type of interaction as "Glu353 $n_O(\pi)$ → EST σ^*_{OH}". The next pair "3" was the CT interaction at the same site, Glu353 $n_O(\sigma)$ → EST σ^*_{OH}, in which the lone-pair orbital on the same oxygen atom had σ-character; the occupation number was 0.0064. The sum of the occupation numbers for the set of these two pairs was 0.022, which suggests strong CT interactions from Glu353 to EST. This amount of transferred electrons (0.022) resulted in −20.7 kcal/mol stabilization of CAFI energy

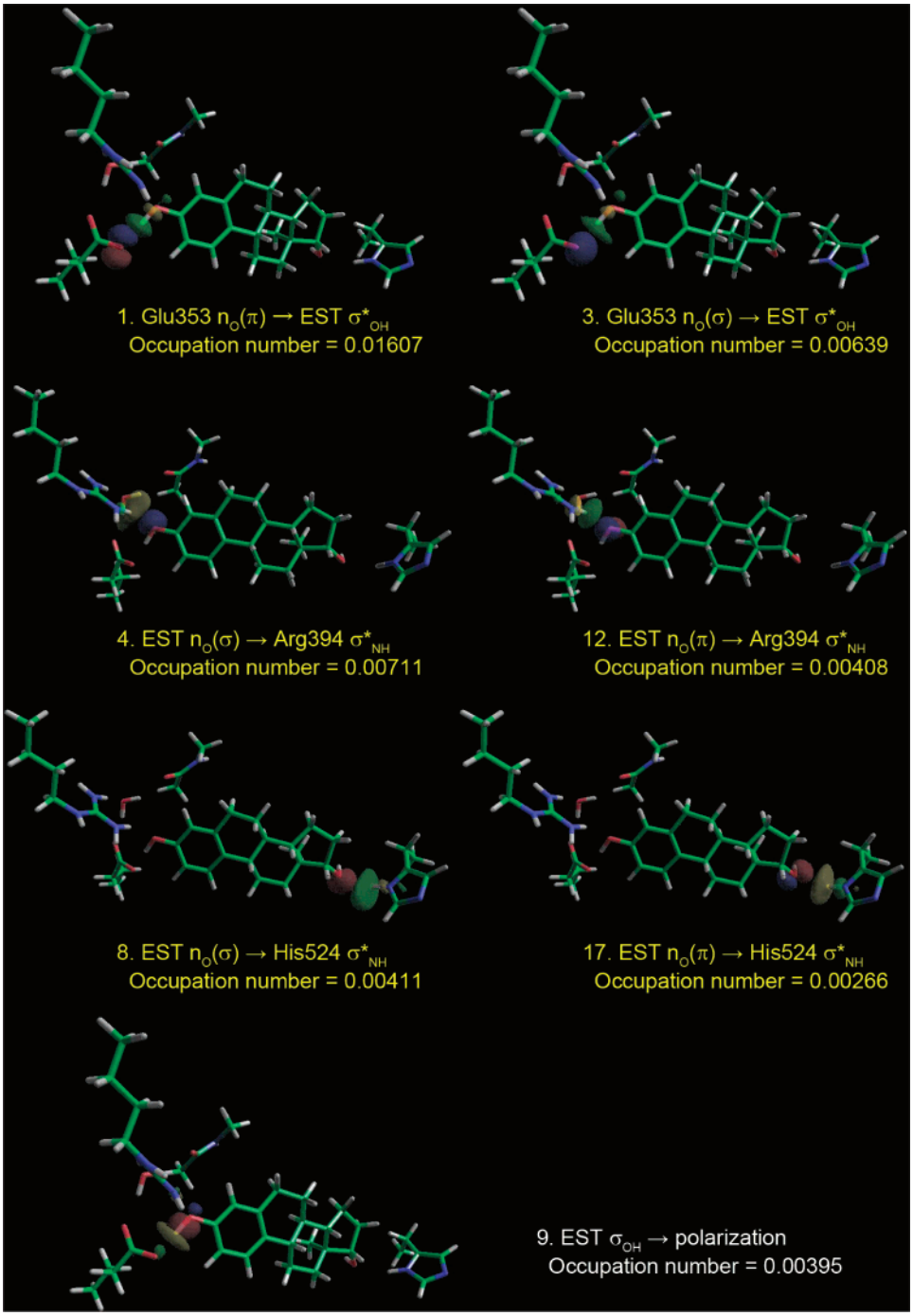

Figure 7. Pairs of "hole orbital" and "particle orbital" concerning CT and POL interactions in the ER−EST complex obtained by the CAFI calculations. The phasing of hole orbital is colored in red and blue. The corresponding colors of the particle orbital are yellow and green, respectively. The title numbers of each pair are sequential serial numbers for natural paired orbital sets in order of the relaxation energies. Occupation numbers as transferred electrons for each pair are also given in each title.

as discussed above, which was comparable with other studies; Reed and Weinhold[31] reported a natural bond orbital analysis of water dimer in which small amounts of CT (0.01 electrons or less) into antibonding orbitals could result in the stabilization of a hydrogen bond by about −10 kcal/mol; our previous CAFI study[25] also suggested similar results for water dimer. The next set was the CT interactions "4" and "12", EST $n_O(\sigma) \rightarrow$ Arg394 σ^*_{NH} and EST $n_O(\pi) \rightarrow$ Arg394 σ^*_{NH}, with occupation numbers of 0.0071 and 0.0041, respectively; the sum of the occupation numbers for the CT interactions from EST to Arg394 was 0.011. The third set was the CT interactions "8" and "17", EST $n_O(\sigma) \rightarrow$ His524 σ^*_{NH} and EST $n_O(\pi) \rightarrow$ His524 σ^*_{NH}, with occupation numbers of 0.0041 and 0.0027, respectively; the sum of the occupation numbers for the CT interactions from EST to His524 was 0.007. The CT interactions of this set were observed at the other hydrogen-bonding site of EST as compared to the former two sets. The POL interaction "9" of the EST σ_{OH} orbital was observed in the EST, and the occupation number was 0.0040. These results clearly show that the major CT interactions were electron donation from Glu353 to EST and that there were considerable CT interactions as the "back-donation" of electrons from the EST to Arg394 and His524.

4. Conclusions

Molecular interactions between the ER and its natural ligand, 17β-estradiol (EST), were calculated and visualized by means

of an ab initio FMO method. All of the significant interactions of EST were found to occur with surrounding residues. Strong electrostatic interactions were observed between the EST and several charged/polarized residues, in particular for Glu353, Arg394, His524, and Thr347. Weak electrostatic interactions and considerable dispersion interactions were observed between the EST and all surrounding hydrophobic residues; the strongest stabilization was found at Phe404, which interacts with EST by perpendicular $\pi-\pi$ stacking. Further, as compared to experimental mutagenesis, "direct" interactions were observed between the ligand and the key residues for the binding function of the ER: Glu353, Leu525, Met528, and His524. Therefore, both interactions with charged/polarized and hydrophobic residues were equally important to the total interaction energies. These findings clearly suggest that dispersion energies play an important role in stabilization and that the inclusion of electron correlation is essential to characterizing ER−ligand interactions.

In addition, CT interactions were found to occur through hydrogen-bond networks between the EST and the strongly interacting residues, i.e., Glu353, Arg394, and His524. The CT interactions from the Glu353 n_O to the EST σ^*_{OH} were particularly strong; those from the EST n_O on the same hydroxyl group to the Arg394 σ^*_{NH} and from the EST n_O on the other hydroxyl group to the His524 σ^*_{NH} were also strong. Such "electron donation" from the ER to the EST and "electron back-donation" from the EST to the ER significantly contributed to their bindings. Therefore, both hydroxyl groups of EST were important as an electron acceptor at one hydrogen-bonding site with Glu353 and as an electron donor at the same site with Arg394 and at the other hydrogen-bonding site with His524 in the ligand-binding pocket of the ER. Together with the findings regarding the electrostatic and dispersion interactions discussed above, such knowledge could be utilized for efficient screening of ligands with high binding affinities to the ER, which is an important factor in drug discovery.

Acknowledgment. The authors thank Dr. Takeshi Ishikawa and Dr. Hirofumi Watanabe for technical assistance. This work was primarily supported by the "Core Research for Evolutional Science and Technology" project of the Japan Science and Technology Agency. A part of this research was also carried out in conjunction with the "Revolutionary Simulation Software" (RSS21) project supported by the Ministry of Education, Culture, Sports, Science, and Technology.

References and Notes

(1) Renaud, J. P.; Moras, D. *Cell. Mol. Life Sci.* **2000**, *57*, 1748−1769.

(2) Steinmetz, A. C. U.; Renaud, J.-P.; Moras, D. *Annu. Rev. Biophys. Biomol. Struct.* **2001**, *30*, 329−359.

(3) Nilsson, S.; Kuiper, G.; Gustafsson, J.-Å. *Trends Endocrinol. Metab.* **1998**, *9*, 387−395.

(4) Sonnenschein, C.; Soto, A. M. *J. Steroid. Biochem. Mol. Biol.* **1998**, *65*, 143−150.

(5) Berman, H. M.; Westbrook, J.; Feng, Z.; Gilliland, G.; Bhat, T. N.; Weissig, H.; Shindyalov, I. N.; Bourne, P. E. *Nucleic Acids Res.* **2000**, *28*, 235−242. The RCSB Protein Data Bank (http://www.rcsb.org/).

(6) Brzozowski, A. M.; Pike, A. C.; Dauter, Z.; Hubbard, R. E.; Bonn, T.; Engström, O.; Öhman, L.; Greene, G. L.; Gustafsson, J.-Å.; Carlquist, M. *Nature* **1997**, *389*, 753−758.

(7) Herynk, M. H.; Fuqua, S. A. W. *Endocr. Rev.* **2004**, *25*, 869−898.

(8) Oostenbrink, C.; van Gunsteren, W. F. *Proc. Natl. Acad. Sci. U.S.A.* **2005**, *102*, 6750−6754.

(9) van Lipzig, M. M.; ter Laak, A. M.; Jongejan, A.; Vermeulen, N. P.; Wamelink, M.; Geerke, D.; Meerman, J. H. *J. Med. Chem.* **2004**, *47*, 1018−1030.

(10) Fukuzawa, K.; Kitaura, K.; Uebayasi, M.; Nakata, K.; Kaminuma, T.; Nakano, T. *J. Comput. Chem.* **2005**, *26*, 1−10.

(11) Kitaura, K.; Sawai, T.; Asada, T.; Nakano, T.; Uebayasi, M. *Chem. Phys. Lett.* **1999**, *312*, 319−324.

(12) Kitaura, K.; Ikeo, E.; Asada, T.; Nakano, T.; Uebayasi, M. *Chem. Phys. Lett.* **1999**, *313*, 701−706.

(13) Nakano, T.; Kaminuma, T.; Sato, T.; Akiyama, Y.; Uebayasi, M.; Kitaura, K. *Chem. Phys. Lett.* **2000**, *318*, 614−618.

(14) Nakano, T.; Kaminuma, T.; Sato, T.; Fukuzawa, K.; Akiyama, Y.; Uebayasi, M.; Kitaura, K. *Chem. Phys. Lett.* **2002**, *351*, 475−480.

(15) ABINIT-MP ver 3.0 is available from the website of RSS21 project http://www.rss21.iis.u-tokyo.ac.jp/en.

(16) Amari, S.; Aizawa, M.; Zhang, J.; Fukuzawa, K.; Mochizuki, Y.; Iwasawa, Y.; Nakata, K.; Chuman, H.; Nakano, T. *J. Chem. Inf. Model.* **2006**, *46*, 221−230.

(17) Nemoto, T.; Fedorov, D. G.; Uebayasi, M.; Kanazawa, K.; Kitaura, K.; Komeiji, Y. *Comput. Biol. Chem.* **2005**, *29*, 434−439.

(18) Fukuzawa, K.; Komeiji, Y.; Mochizuki, Y.; Kato, A.; Nakano, T.; Tanaka, S. *J. Comput. Chem.* **2006**, *27*, 948−960.

(19) Mochizuki, Y.; Nakano, T.; Koikegami, S.; Tanimori, S.; Abe, Y.; Nagashima, U.; Kitaura, K. *Theor. Chem. Acc.* **2004**, *112*, 442−452.

(20) Mochizuki, Y.; Koikegami, S.; Nakano, T.; Amari, S.; Kitaura, K. *Chem. Phys. Lett.* **2004**, *396*, 473−479.

(21) Fedorov, D. G.; Kitaura, K. *J. Chem. Phys.* **2004**, *121*, 2483−2490.

(22) Yamagishi, K.; Yamamoto, K.; Yamada, S.; Tokiwa, H. *Chem. Phys. Lett.* **2006**, *420*, 465−468.

(23) Yamagishi, K.; Yamamoto, K.; Mochizuki, Y.; Nakano, T.; Yamada, S.; Tokiwa, H., to be published.

(24) Mochizuki, Y. *Chem. Phys. Lett.* **2005**, *410*, 165−171.

(25) Mochizuki, Y.; Fukuzawa, K.; Kato, A.; Tanala, S.; Kitaura, K.; Nakano, T. *Chem. Phys. Lett.* **2005**, *410*, 247−253.

(26) Frisch, M. J.; Trucks, G. W.; Schlegel, H. B.; Scuseria, G. E.; Robb, M. A.; Cheeseman, J. R.; Montgomery, J. A., Jr.; Vreven, T.; Kudin, K. N.; Burant, J. C.; Millam, J. M.; Iyengar, S. S.; Tomasi, J.; Barone, V.; Mennucci, B.; Cossi, M.; Scalmani, G.; Rega, N.; Petersson, G. A.; Nakatsuji, H.; Hada, M.; Ehara, M.; Toyota, K.; Fukuda, R.; Hasegawa, J.; Ishida, M.; Nakajima, T.; Honda, Y.; Kitao, O.; Nakai, H.; Klene, M.; Li, X.; Knox, J. E.; Hratchian, H. P.; Cross, J. B.; Adamo, C.; Jaramillo, J.; Gomperts, R.; Stratmann, R. E.; Yazyev, O.; Austin, A. J.; Cammi, R.; Pomelli, C.; Ochterski, J. W.; Ayala, P. Y.; Morokuma, K.; Voth, G. A.; Salvador, P.; Dannenberg, J. J.; Zakrzewski, V. G.; Dapprich, S.; Daniels, A. D.; Strain, M. C.; Farkas, O.; Malick, D. K.; Rabuck, A. D.; Raghavachari, K.; Foresman, J. B.; Ortiz, J. V.; Cui, Q.; Baboul, A. G.; Clifford, S.; Cioslowski, J.; Stefanov, B. B.; Liu, G.; Liashenko, A.; Piskorz, P.; Komaromi, I.; Martin, R. L.; Fox, D. J.; Keith, T.; Al-Laham, M. A.; Peng, C. Y.; Nanayakkara, A.; Challacombe, M.; Gill, P. M. W.; Johnson, B.; Chen, W.; Wong, M. W.; Gonzalez, C.; Pople, J. A. *Gaussian 03*, revision C.02; Gaussian, Inc.: Wallingford, CT, 2004.

(27) BioStation Viewer ver 6.00 is available from the website of RSS21 project http://www.rss21.iis.u-tokyo.ac.jp/en.

(28) Jurecka, P.; Hobza, P. *Chem. Phys. Lett.* **2002**, *365*, 89−94.

(29) Pittner, J.; Hobza, P. *Chem. Phys. Lett.* **2004**, *390*, 496−499.

(30) Vondrasek, J.; Bendova, L.; Klusak, V.; Hobza, P. *J. Am. Chem. Soc.* **2005**, *127*, 2615−2619.

(31) Reed, A. E.; Weinhold. F. *J. Chem. Phys.* **1983**, *78*, 4066−4073.